Local and Global Active Contour Model for Image Segmentation With Intensity Inhomogeneity

QING CAI [1,2] **, HUIYING LIU**[1]**, YIMING QIAN**[2]**, (Student Member, IEEE), JING LI**[3]**,**
XIAOJUN DUAN[4]**, (Member, IEEE), AND YEE-HONG YANG**[2]**, (Senior Member, IEEE)**
[1]School of Automation, Northwestern Polytechnical University, Xi'an 710072, China
[2]Department of Computing Science, University of Alberta, Edmonton, AB T6G 2E8, Canada
[3]School of Mechanical Engineering, Northwestern Polytechnical University, Xi'an 710072, China
[4]National Key Laboratory of UVA Technology, Northwestern Polytechnical University, Xi'an 710072, China

Corresponding authors: Qing Cai (caiqing@mail.nwpu.edu.cn) and Xiaojun Duan (duanxiaojun@nwpu.edu.cn)

This work was supported in part by the National Science Foundation of China under Grant 51705424 and Grant 61473219, in part by the Major Projects of Basic Scientific Research under Grant JCKY2016204A601, in part by the Natural Sciences and Engineering Research Council of Canada, and in part by the University of Alberta.

ABSTRACT The active contour model (ACM) is a popular approach for image segmentation. Many existing ACMs perform poorly in severe inhomogeneous images. To address this issue, a novel local and global ACM (LaG_ACM) is proposed in this paper. First, we define a global fitting image formulation that encodes the global property of an image and a global energy term using the relative entropy between the original image and the proposed global fitting image formulation. Then, a local image bias field formulation is defined to extract the local image information and to estimate the bias field. By integrating the proposed local image bias field formulation with the ACM, we specify a local energy term using the mean squared error to accommodate severe inhomogeneous images. More importantly, we define an adaptive weighting function using image entropy, which can automatically adjust the weight between the local and global energy terms according to the degree of intensity inhomogeneity. Finally, the experimental results on images with different degrees of intensity inhomogeneity validate the favorable performance of the LaG_ACM.

INDEX TERMS Active contour model, image segmentation, intensity inhomogeneity, local and global energy term, adaptive weighting function.

I. INTRODUCTION

IMAGE segmentation is a challenging task in computer vision and plays a crucial role in numerous real-world applications, such as video surveillance [1], object tracking [2]–[4], remote sensing image segmentation [5]and medical imaging [6]–[10]. Intensity inhomogeneity caused by imaging conditions and imaging devices is one of the biggest challenges for image segmentation since it seriously affects the segmentation accuracy. In order to address this issue, many methods have been proposed, in which the active contour model (ACM) [11]–[16], a framework in computer vision for delineating an object outline, has shown effectiveness, especially for inhomogeneous grayscale images. Existing ACMs can be broadly divided into two categories: the edge-based ACMs and the region-based ACMs. The edge-based ACMs [17]–[26] define the energy function using image gradients, and are usually applied to segment images with strong edges. For example, the geodesic

active contour model [17] and the distance regularized level set evolution (DRLSE) model [22]. However, this kind of ACMs is sensitive to noise, and may fail in segmenting images with weak edges and complex backgrounds. To address this problem, the region-based ACMs [27]–[35] are proposed utilizing region information rather than gradients to define the energy function. Examples include the Mumford-Shah model [27], the Chan-Vese (CV) model [29] and the multi-phase model [31]. Even though these models can guide the evolving curve to stop at weak boundaries that cannot be detected by the edge-based ACMs, they may fail to segment inhomogeneous images because of the homogeneous assumption in each region.

To solve this problem, the local region-based ACMs [36]–[48] are proposed, with an energy function defined based on assuming that the image intensity is inhomogeneous in a global region but homogeneous in a small local region. Representative methods in this category

include the local binary fitting (LBF) model [36], the local Gaussian distribution fitting (LGDF) model [38], the local Chan-Vese (LCV) model [39], the local image fitting (LIF) model [40], the local region-based Chan-Vese model [41] and the locally linear classification model [42], etc. In particular, the LBF model proposed by Li *et al.* [36] has attracted extensive attention for its good performance in slightly inhomogeneous images by embedding the local image intensity information in the CV model. The LIF model proposed by Zhang *et al.* [40] using the defined local image fitting energy to model local image intensity. Unfortunately, most of them are not robust to noise and to initialization than the global region-based models because of using only local information to construct the energy function. Besides, these models perform poorly in severe inhomogeneous images.

Recently, a wide variety of hybrid ACMs, incorporating two models into an energy function, are proposed. The local and global ACMs [9], [49]–[58] are their typical representatives, which define the energy function by combining the global energy term and the local energy term using a weight coefficient, and achieve tremendous success in inhomogeneous intensity image segmentation. For example, Wang *et al.* [49] propose the local and global intensity fitting (LGIF) model by combining the data terms of the CV model and the LBF model. Yu *et al.* propose the local and global fitting energy dynamically (LaG_FED) model in [50] by defining an entropy based weight function to adjust the weight between two terms. In [53], Wang *et al.* propose the local and global Gaussian distribution fitting (GARAC) model using the local and global Gaussian distributions with different means and variances. But the two models both use a fixed weight coefficient to adjust the contributions of the local and the global terms, which limits their performance in segmenting inhomogeneous intensity images. Zhou *et al.* [9] propose the local and global intensity information (LaG_II) model by constructing a weighting function that adaptively adjusts the weight to improve the performance in medical image segmentation. The other representatives of the hybrid ACMs are the bias field corrected ACMs [8], [10], [59]–[63], such as the local intensity clustering (LIC) model [60] and the multiplicative intrinsic component optimization (MICO) model [61], the correntropy-based level set method (CB_LSM) [8], the statistical level set approach (SLSA) [63] and the adaptive-scale active contour model (ASACM) [10].

Although tremendous success has been achieved in inhomogeneous image segmentation, it is still a conundrum for ACMs to segment images with severe intensity inhomogeneity since the noise, initialization and complex background all can affect the final segmentation result. In this paper, we propose a novel local and global ACM (LaG_ACM) for segmenting images with severe intensity inhomogeneity. Specifically, we first define a global image fitting formulation to extract the image global information, and then propose a new global energy term based on the relative entropy (also called Kullback_Leibler divergence) between the original image

and the global fitting image formulation. Then, we define a local image bias field formulation by incorporating a bias field corrected model into the ACM and propose a local energy term based on the mean squared error. In addition, we define a weighting function based on image entropy that is related to our previous work [10]. In this paper, we use image entropy to define a weighting function, but in [10], image entropy is used to define an adaptive-scale operator. In particular, the weighting function defined in this paper is used to adjust the weight between local term and global term, which avoids the disadvantage of our previous method [10], which only adjusts the local scale of the energy term using an adaptive-scale operator (see the comparison experiment between the two model in Secion IV-C5). Finally, the experimental results on different degrees of inhomogeneous intensity images, such as synthetic images, natural images, medical images, remote sensing images, infrared images and sonar images, validate the feasibility and effectiveness of the proposed LaG_ACM. Furthermore, the experimental results on severe inhomogeneous intensity images show that the proposed method outperforms the state-of-the-art methods.

Briefly, the contributions of this paper include:

- A novel global energy term is defined using the relative entropy between the original image and the propose global image fitting formulation, which improves the robustness to noise and to initialization, as well as the segmentation efficiency of the LaG_ACM.

- A new local image bias field formulation is defined by incorporating the bias field model into the active contour model to simultaneously extract the local image intensity information and to estimate the bias field. As a result, it improves the segmentation accuracy for severe inhomogeneous images.

- A novel weighting function is constructed using image entropy that can adaptively adjust the weight between the local and the global terms according to the degree of intensity inhomogeneity. Thus, it accelerates the convergence of the evolving curve and hence the speed of segmentation.

The rest of the paper is organized as follows: In Section II, we review three related models and discuss their advantages and disadvantages. In Section III, we propose our method. In Section IV, we validate our method by various experiments on different kind of images with intensity inhomogeneity. Section V concludes the paper.

II. BACKGROUND AND RELATED WORK
A. CHAN-VESE (CV) MODEL
In [29], Chan *et al.* propose the CV model by assuming that the image intensity inside and outside of the evolving curve are homogeneous. The energy function is defined as:

$$E^{CV} = \sum_{i=1}^{2} \lambda_i \int_{\Omega} |I(x) - c_i|^2 M_i(\phi) \, dx$$

$$+ u \int_{\Omega} \delta(\phi) |\nabla \phi| \, dx + v \int_{\Omega} H(\phi) \, dx, \quad (1)$$

where $\lambda_i(i = 1, 2)$, u and v are balancing factors controlling the weights of different terms. $c_i(i = 1, 2)$ are constants describing the image intensity inside and outside the evolving curve. $M_1(\phi) = H(\phi)$, and $M_2(\phi) = 1 - H(\phi)$ are the membership functions of the background and the foreground, respectively. $H(\phi)$ and $\delta(\phi) = \frac{d}{d\phi}H(\phi)$ are the Heaviside function and the Dirac delta function, respectively. ϕ is the level set function. $I(x)$ denotes the value of pixel x. Using image intensity information rather than boundary gradient, the CV model can accurately segment images with weak edges and noise. However, it performs poorly in images with intensity inhomogeneity because the constant $c_i(i = 1, 2)$ cannot model local intensity distributions of an image.

B. LOCAL INTENSITY CLUSTERING (LIC) MODEL
In [60], Li *et al.* propose the LIC model based on a local clustering criterion function, which can simultaneously segment an inhomogeneous image and estimate its bias field. The two-phase energy function is defined as:

$$E^{LIC} = \sum_{i=1}^{2} \int \int K(y - x)|I(x) - b(y)c_i|^2 M_i(\phi(x))dxdy$$
$$+ u \int_\Omega \frac{1}{2}(|\nabla\phi| - 1)^2 \, dx + v \int_\Omega |\nabla H(\phi)| \, dx, \quad (2)$$

where K is the truncated Gaussian function to control the size of the local neighborhood. $c_i(i = 1, 2)$ represent intensity in the local neighborhood. $b(y)$ is the bias field accounting for intensity inhomogeneity of pixel y. The second and the third terms are the penalty term and the length regularization term, and u, v are their balancing factors, respectively.

Due to the local clustering criterion function, the LIC model performs favorably in slightly inhomogeneous images. But it may fail to segment severe inhomogeneous images since its function is sensitive to the initial contours. In particular, it often converges to non-unique local minima, and the resulting contour may settle in areas with severe inhomogeneity instead of the real boundaries. Besides, its penalty term exhibits unstable behavior, which is described in Section III-A4.

C. LOCAL AND GLOBAL INTENSITY FITTING (LGIF) MODEL
In [49], Wang *et al.* propose the LGIF by incorporating the CV model and the LBF model into one energy function using a fixed weight. The two-phase energy function is defined as:

$$E^{LGIF} = \omega \sum_{i=1}^{2} \lambda_i \int |I(x) - c_i|^2 M_i(\phi(x))dxdy$$
$$+ (1 - \omega) \sum_{i=1}^{2} \int \int K_\sigma(x - y)|I(y) - f_i(x)|^2$$
$$\times M_i(\phi(y))dxdy + u \int_\Omega \frac{1}{2}(|\nabla\phi(x)| - 1)^2 \, dx$$
$$+ v \int_\Omega |\nabla H(\phi(x))| \, dx, \quad (3)$$

where ω is a weight that controls the contributions of the first two terms. K_σ is a Gaussian kernel with standard deviation σ. $f_i(x)(i = 1, 2)$ are two functions that fit local image intensities near the point x inside and outside of the evolving curve, respectively.

The LGIF model produces significant improvement in inhomogeneous intensity image segmentation, because it avoids the disadvantages that the CV model has in segmenting images with intensity inhomogeneity and the LBF model has in its poor robustness to noise and to initialization, but retains the advantages that the CV model has in its robustness to noise and to initialization and the advantages that the LBF model has in segmenting images with intensity inhomogeneity. Nevertheless, it cannot segment severe inhomogeneous images with complex background because of using a fixed weight and the inherent defects of the CV model and the LBF model.

III. PROPOSED METHOD
In this section, we describe the proposed method LaG_ACM. Its architecture is shown in Fig. 1.

A. ENERGY TERM
The energy function of the proposed method is defined as:

$$E^{LaG\_ACM} = (1 - \Psi)E^G + \Psi E^L + E^R, \quad (4)$$

where Ψ is the adaptive weighting function. E^G, E^L and E^R are the global energy term, the local energy term and the regularization term, respectively. The detailed definition of each term is described in the following subsections.

1) GLOBAL ENERGY TERM
The purpose of segmentation is to find the best partition of image I, so we define a global fitting image (GFI) formulation I^{GFI} to fit the original image I. Let $\Omega = \{\Omega_1 \cup \Omega_2 \cup, \cdots, \cup\Omega_N\}$ be the image domain, where $\Omega_i \cap \Omega_j = \emptyset$ for $i \neq j$, $I = \cup_{i=1}^{N}\Omega_i$ and Ω_i denotes the ith partition of image I. For the two-phase case, Ω is divided into $\Omega_1(\phi \geq 0)$ and $\Omega_2(\phi \leq 0)$, respectively, and the global image fitting formulation is defined as:

$$I^{GFI}(x) = \sum_{i=1}^{2} c_i M_i(\phi(x)), \quad (5)$$

where $c_i(i = 1, 2)$ is the average intensity of the ith object region. ϕ is the level set function and $\phi = 0$ is the zero level set of the evolving curve. $M_1(\phi) = H(\phi)$ and $M_2(\phi) = 1 - H(\phi)$ are membership functions of each region. $H(\phi)$ is the Heaviside function and is defined as:

$$H(\phi) = \begin{cases} 1, & \text{if } \phi \leq 0 \\ 0, & \text{if } \phi \geq 0. \end{cases} \quad (6)$$

Based on relative entropy, a difference measure operator, the global energy term is defined as:

$$E^G = \int_\Omega \left(I(x)\log\frac{I(x)}{I^{GFI}(x)} + I^{GFI}(x)\log\frac{I^{GFI}(x)}{I(x)} \right) dx. \quad (7)$$
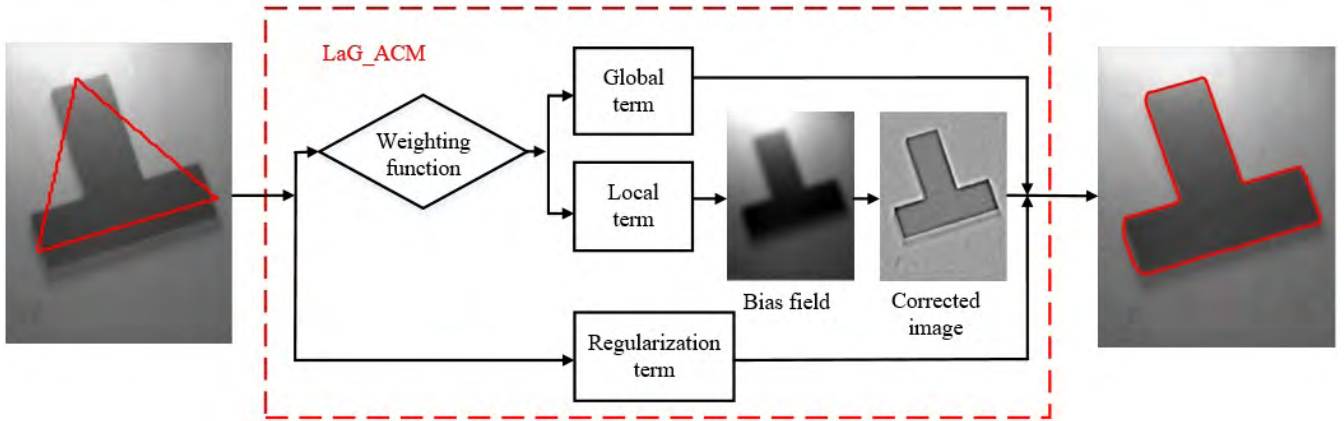
FIGURE 1. Illustration of the architecture of the LaG_ACM. By using image entropy, the weighting function first adaptively adjusts the weight between the local and the global terms based on the inhomogeneous image intensity. Then the global term accelerates the evolving curve to the boundary and the local term estimates the bias field and extracts the local intensity information. Finally, the LaG_ACM finishes the segmentation for the image with intensity inhomogeneity under the effect of the regularization term.
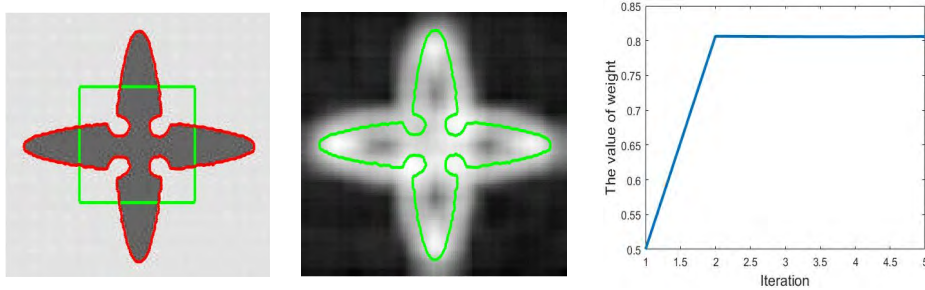

FIGURE 2. Illustration of the weighting function. From left to right: (left) the initial contour (the green line) and the final segmentation result (the red line) in the original image, (middle) the final contour in the local entropy image, (right) the value of the weighting function Ψ during segmentation.

2) LOCAL ENERGY TERM

An inhomogeneous intensity image consists of an object, background and a bias field. If we can accurately estimate the bias field, the issue of inhomogeneous intensity image segmentation can be addressed by subtracting the bias field. Inspired by this observation, we define a local image bias field (LIBF) formulation to estimate the bias field, which assumes that the bias field in the image domain is slowly changing, and the intensity in a local neighborhood is constant. That is:

$$I^{LIBF}(x) = w(x, y) \sum_{i=1}^{2} b(y)\theta_i M_i(\phi(x)), \quad (8)$$

where $w(u) = \beta e^{-|u|^2/2\sigma^2}$ ($|u| \le \gamma$, γ denotes the local neighborhood radius, and β the normalization constant), is a truncated Gaussian function controlling the local neighborhood of the local image bias field. b denotes the bias field. θ_i denotes the average intensity of the local neighborhood of the ith region Ω_i. Based on the mean squared error, the local energy term is defined as:

$$E^L = \frac{1}{2} \int \int |I(x) - I^{LIBF}(x)|^2 \, dxdy. \quad (9)$$

3) WEIGHTING FUNCTION

As mentioned in Section I, the weight in the hybrid model plays an important role in the segmentation accuracy and efficiency. In this section, we define a novel weighting function using image entropy. Fig. 2, is a synthetic image with intensity homogeneity, and the intensity changes greatly across the boundary. At the beginning of evolution, the local entropy near the evolving curve is relatively small. As a result, the weight is small and the global energy term plays the main role to accelerate the curve moving towards the boundary. With the propagation of the curve to the edge, the weight increases as shown in the right image and the local energy term gradually plays the main role to extract the local image intensity. The weighting function Ψ is defined as:

$$\Psi = \text{mean}\left(\frac{\xi - \min(\xi)}{\max(\xi) - \min(\xi)}\right) \in [0, 1], \quad (10)$$

where mean denotes the mean operator. ξ is the local entropy, and is defined as:

$$\xi = - \int_{x \in \{\phi(x)=0\}} \rho(x)\log\rho(x) \, dx, \quad (11)$$

where ρ denotes the intensity of point x in Ω_x.

4) REGULARIZATION TERM

In order to ensure stable evolution of the level set and to avoid complex and time-consuming re-initialization, a regularization term is indispensible to the ACM, and is defined as:

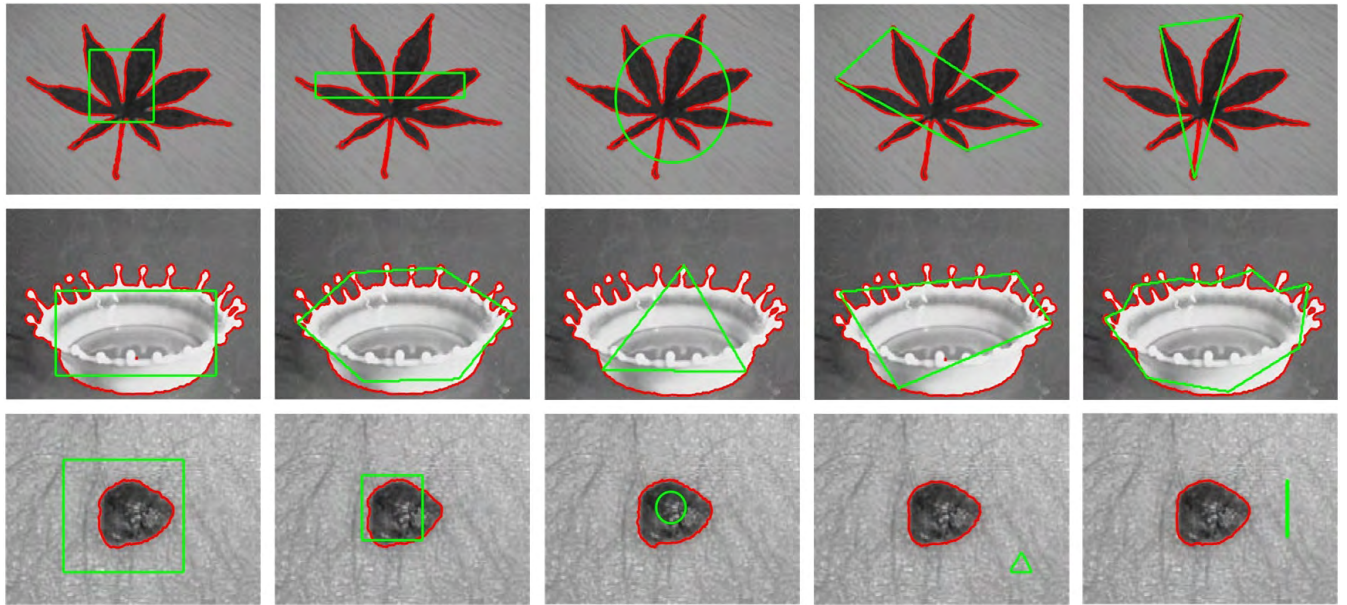$$E^R = v \int_{\Omega} |\nabla H(\phi)| \, dx + u \int_{\Omega} p(|\nabla \phi|) \, dx, \quad (12)$$

FIGURE 3. Segmentation results by the proposed method with different initializations. The green lines and red lines denote the initial contours and the final segmentation results, respectively.

where u and v are the balancing factors. The first term is the length regularization term, playing the role to suppress small isolated region in the final results. The second term is the penalty term to avoid the re-initialization procedure, and $p(s)$ is the energy density. Using the traditional penalty term, a ACM often exhibits unstable behavior as mentioned in Section II-B since the diffusion rate $d_p(s) = \frac{p'(s)}{s} = 1 - \frac{1}{s}$ approaches ∞ when $s \to 0$ [22]. To address this issue, we propose a double-well piecewise polynomial, which is defined as:

$$p(s) = \begin{cases} \frac{1}{2}s^2(s-1)^2, & \text{if } s \leq 1 \\ \frac{1}{2}(s-1)^2, & \text{if } s \geq 1. \end{cases} \quad (13)$$

$d_p(s)$ is the diffusion rate defined as:

$$d_p(s) = \frac{p'(s)}{s} = \begin{cases} (s-1)(2s-1), & \text{if } s \leq 1 \\ 1 - \frac{1}{s}, & \text{if } s \geq 1. \end{cases} \quad (14)$$

From the above two equations, we can see that the novel penalty term completely avoids the unstable issue because the diffusion rate $d_p(s) = 1$ instead of $d_p(s) \to \infty$ when $s \to 0$.

B. LEVEL SET FORMULATION AND IMPLEMENTATION

To complete the final segmentation, the level set implementation and numerical implementation are needed to minimize the LaG_ACM, and they are described next.

1) TWO-PHASE LEVEL SET IMPLEMENTATION

For the two-phase case, the image domain is divided into two disjoint regions using one level set ϕ only, and the energy

---

Algorithm 1 The Algorithm of LaG_ACM

Input:
    Read in the image to be segmented and initialize the level set function $\phi^0 = \phi_0$.

Initialization:
    Set the values of standard deviation of the truncated Gaussian function σ, coefficients μ, v, time-step Δt, grid spacing interval h, ε, stop condition coefficients ξ and number of iteration termination m.

Repeat:
    1. Compute the weighting function according to Eq. 10 and Eq. 11;
    2. Compute c_i, b, θ_i according to Eq. 19 to Eq. 21 or Eq. 28 to Eq. 30;
    3. Compute H_ε and δ_ε according to Eq. 31 and Eq. 32;
    4. Update the formulas according to Eq. 16 to Eq. 18 or Eq. 25 to Eq. 27;

Until: $(|L(\phi^{i+1}) - L(\phi^i)| < \xi)$ or the number of iterations is equal to m.

Output:
    The final segmentation contour $\phi = \phi^{i+1}$.

---

function is defined as:

$$\begin{aligned} E^{LaG\_ACM} &= (1 - \Psi) \int_\Omega \left(I(x)\log\frac{I(x)}{I^{GFI}(x)} \right. \\ &\quad \left. + I^{GFI}(x)\log\frac{I^{GFI}(x)}{I(x)} \right) dx \\ &\quad + \Psi \frac{1}{2} \int \int |I(x) - I^{LIBF}(x)|^2 \, dxdy \\ &\quad + v \int_\Omega |\nabla H(\phi)| \, dx + u \int_\Omega p(|\nabla\phi|) \, dx. \quad (15) \end{aligned}$$
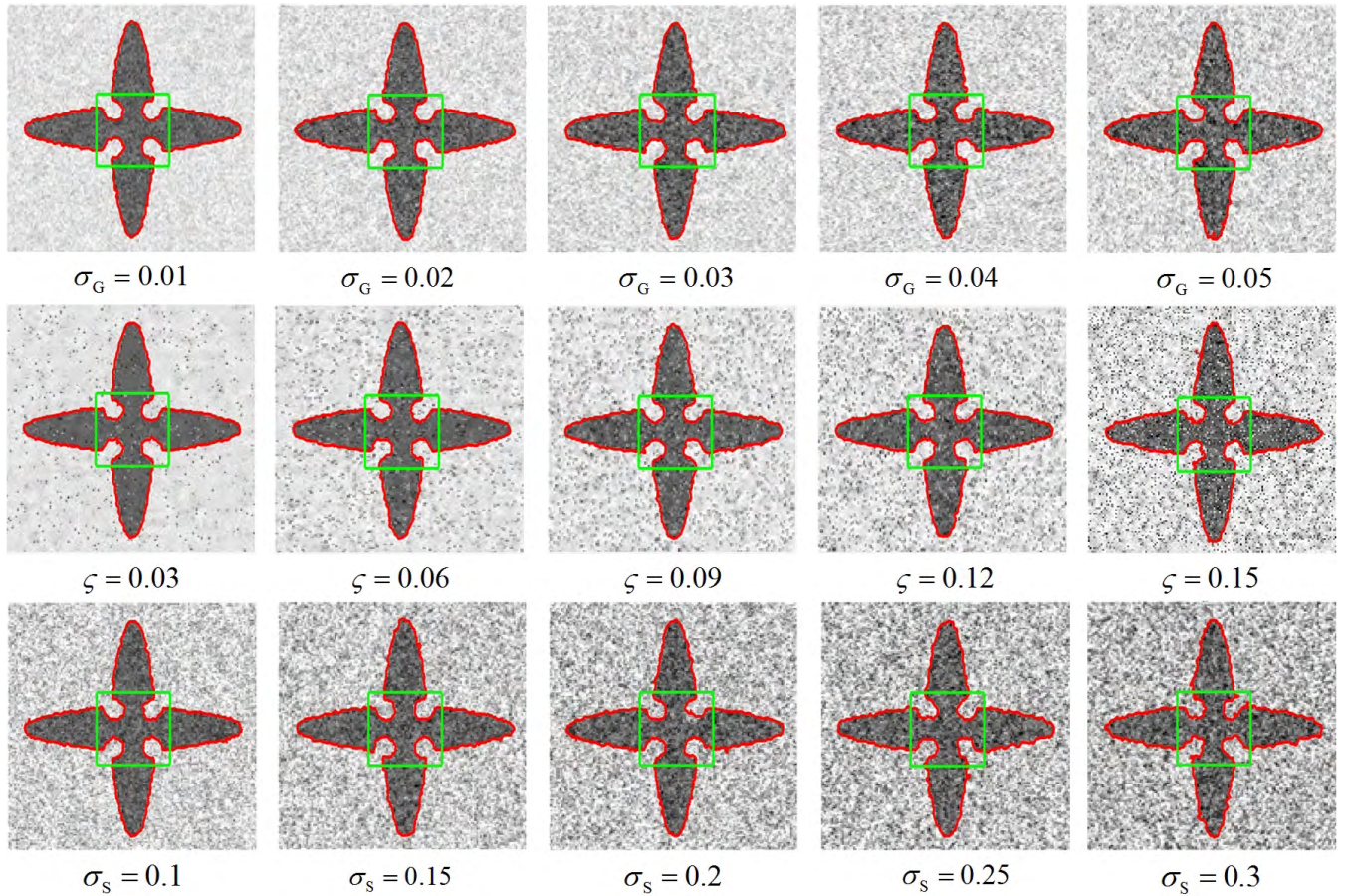
FIGURE 4. Segmentation results of our method with different noise distributions. Row 1: Gaussian white noise with zero mean and different variances ($\sigma_G = 0.01, 0.02, 0.03, 0.04, 0.05$). Row 2: Salt and pepper noise with different noise densities ($\varsigma = 0.03, 0.06, 0.09, 0.12, 0.15$). Row 3: Speckle noise with zero mean and different variances ($\sigma_S = 0.1, 0.15, 0.2, 0.25, 0.3$). We use the Matlab built-in function "imnoise" to add these noises to the original image.

Using the Euler-Lagrange equation and gradient descent flow, and keeping all the parameters fixed and minimizing the above equation with respect to ϕ, we get the iteration formulation (see Appendix for derivation):

$$\frac{\partial \phi}{\partial t} = \delta(\phi)((1-\Psi)\alpha_1 + \Psi\alpha_2) + \nu\delta(\phi)\mathrm{div}\left(\frac{\nabla\phi}{|\nabla\phi|}\right)$$
$$+ u\mathrm{div}(d_p(|\nabla\phi|)\nabla\phi), \qquad (16)$$

$$\alpha_1 = \left(\frac{I(x)}{I^{GFI}(x)} - 1 - \log\frac{I^{GFI}(x)}{I(x)}\right)(c_1 - c_2), \qquad (17)$$

$$\alpha_2 = (I(x) - I^{LIBF}(x))(\theta_1 - \theta_2)(b \otimes w), \qquad (18)$$

where $\delta(\phi) = \frac{dH(\phi)}{d\phi}$ is the Dirac delta function as mentioned in Section II-A. div denotes the divergence operator, and $d_p(s)$ the diffusion rate mentioned above. $\otimes$ represents the convolution operator.

Similarly, keeping ϕ fixed and minimizing with respect to parameters c_i, b, θ_i, we get the update formulas of the parameters as follows:

$$c_i = \frac{\int_\Omega IM_i(\phi)\,dxdy}{\int_\Omega M_i(\phi)\,dxdy}, \qquad (19)$$

$$\theta_i = \frac{\int_\Omega (w \otimes b)IM_i(\phi)\,dy}{\int_\Omega (w^2 \otimes b^2)M_i^2(\phi)\,dy}, \qquad (20)$$

and

$$b = \frac{\left(\sum_{i=1}^{2} I\theta_i M_i(\phi)\right) \otimes w}{\left(\sum_{i=1}^{2} \theta_i^2 M_i^2(\phi)\right) \otimes w^2}. \qquad (21)$$

2) MULTI-PHASE LEVEL SET IMPLEMENTATION

It is difficult for a two-phase level set method to segment multi-object intensity image since the two-phase case can only divide the intensity into two categories: object and background. Thus, for multi-object images with intensity inhomogeneity, such as in brain Magnetic Resonance Images (MRI), the multi-phase level set implementation is indispensable. In particular, the image domain Ω is divided into N ($N > 2$) disjointed regions $\{\Omega_i\}_{i=1}^{N}$ using k level set functions $\Phi = \{\phi_j\}_{j=1}^{k}$ (usually $k = \log_2 N$), and the energy function
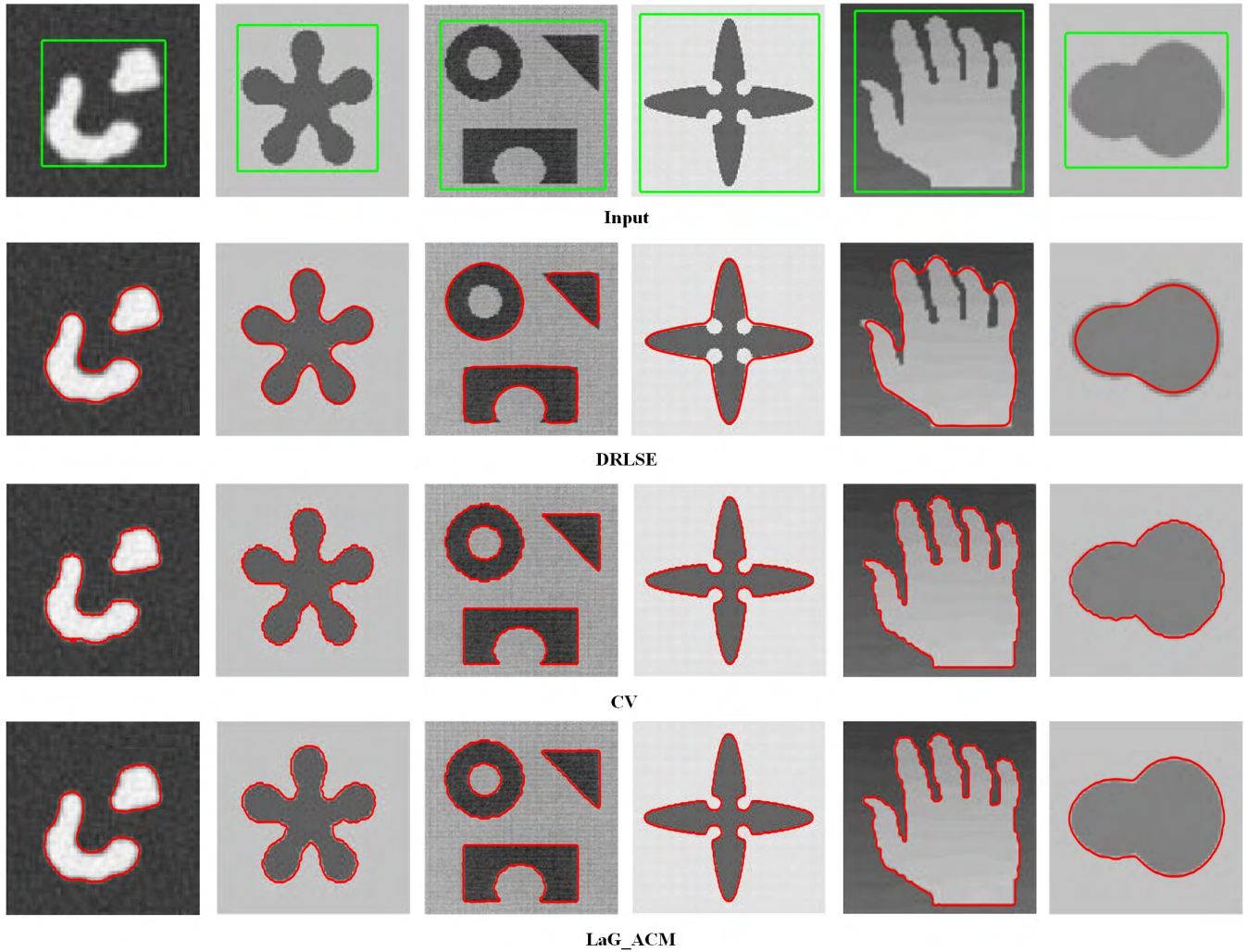
FIGURE 5. Segmentation results for synthetic images. From top to bottom: original images with corresponding initial contours (the green lines), the final segmentation results (the red lines) of the DRLSE [22], the CV [29] and the LaG_ACM, respectively.

is defined as:

$$
\begin{aligned}
E^{LaG\_ACM} &= (1 - \Psi) \int_{\Omega} \left(I(x)\log\frac{I(x)}{I^{GFI}(x)} \right. \\
&\quad \left. + I^{GFI}(x)\log\frac{I^{GFI}(x)}{I(x)} \right) dx. \\
&\quad + \Psi \frac{1}{2} \int \int |I(x) - I^{LIBF}(x)|^2 \, dxdy \\
&\quad + v \sum_{j=1}^{k} \int_{\Omega} |\nabla H(\Phi)| \, dx \\
&\quad + u \sum_{j=1}^{k} \int_{\Omega} p(|\nabla \Phi|) \, dx,
\end{aligned}
\tag{22}
$$

where I^{GFI} and I^{LIBF} are changed to:

$$
I^{GFI}(x) = \sum_{i=1}^{N} c_i M_i(\Phi(x)),
\tag{23}
$$

$$
I^{LIBF}(x) = w(x, y) \sum_{i=1}^{N} b(y)\theta_i M_i(\Phi(x)).
\tag{24}
$$

The minimization of the multi-phase LaG_ACM is similar to that of the two-phase case. Based on the gradient descent flow and the Euler-Lagrange equation, the final iteration equation is:

$$
\begin{aligned}
\frac{\partial \phi_j}{\partial t} &= \delta(\phi_j)((1 - \Psi)\alpha_1 + \Psi \alpha_2) + v \sum_{j=1}^{k} \delta(\phi_j)\mathrm{div}\left(\frac{\nabla \phi_j}{|\nabla \phi_j|} \right) \\
&\quad + u \sum_{j=1}^{k} \mathrm{div}(d_p(|\nabla \phi_j|)\nabla \phi_j),
\end{aligned}
\tag{25}
$$

where α_1, α_2, c_i, b and θ_i are computed as:

$$
\alpha_1 = \left(\frac{I(x)}{I^{GFI}(x)} - 1 - \log\frac{I^{GFI}(x)}{I(x)} \right) \frac{\partial I^{GFI}}{\partial \phi_i},
\tag{26}
$$

$$
\alpha_2 = (I(x) - I^{LIBF}(x))\frac{\partial I^{LIBF}}{\partial \phi_i},
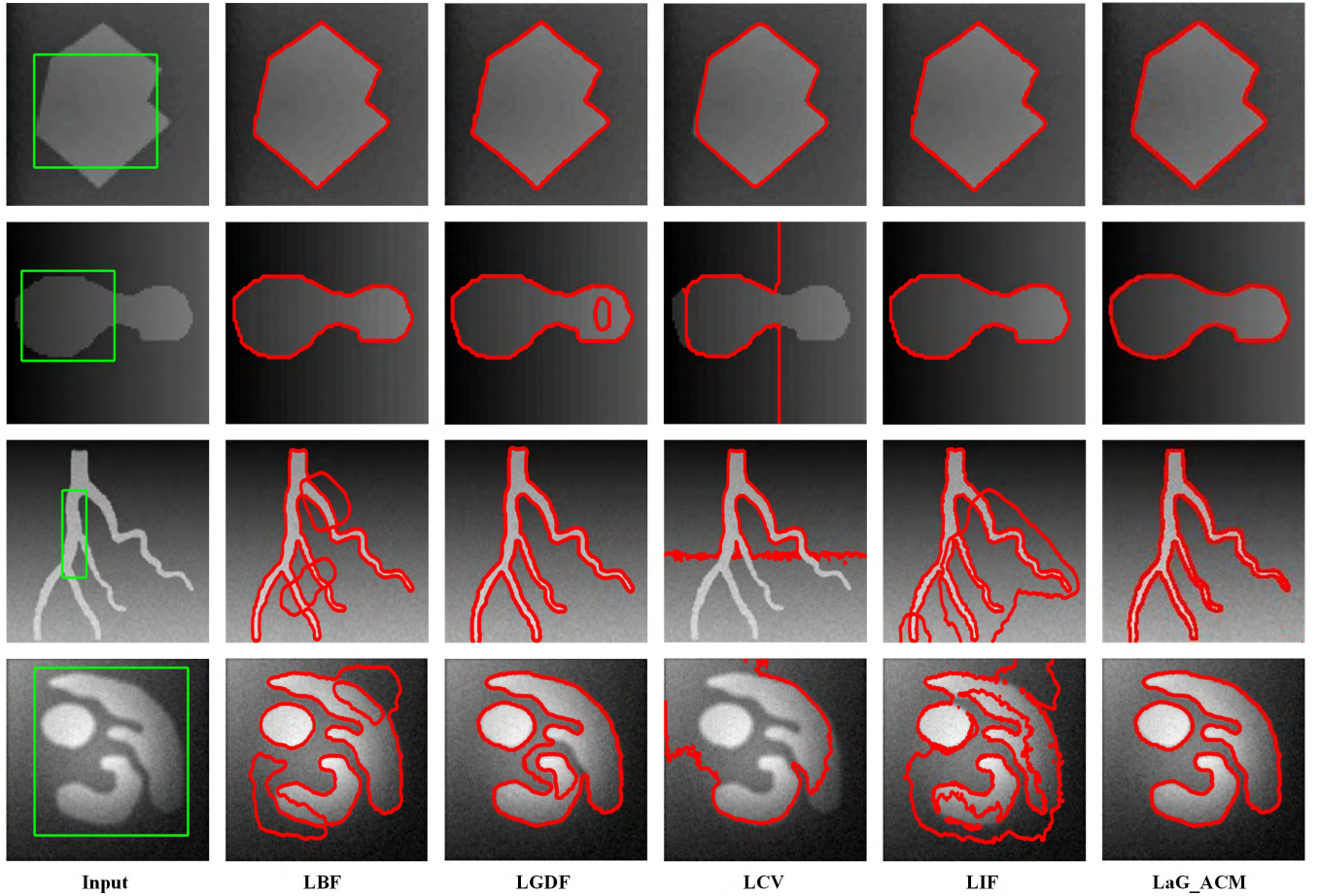\tag{27}
$$

FIGURE 6. Segmentation results for synthetic images with different degrees of intensity inhomogeneity. From left to right: original images with corresponding initial contours (the green lines), segmentation results using the LBF [36], the LGDF [38], the LCV [39], the LIF [40] and the LaG_ACM, respectively.

$$c_i = \frac{\int_\Omega IM_i(\Phi)\,dxdy}{\int_\Omega M_i(\Phi)\,dxdy}, \tag{28}$$

$$\theta_i = \frac{\int_\Omega (w \otimes b)IM_i(\Phi)\,dy}{\int_\Omega (w^2 \otimes b^2)M_i^2(\Phi)\,dy}, \tag{29}$$

$$b = \frac{\left(\sum_{i=1}^{N} I\theta_i M_i(\Phi)\right) \otimes w}{\left(\sum_{i=1}^{N} \theta_i^2 M_i^2(\Phi)\right) \otimes w^2}, \tag{30}$$

where the membership function $M_i(\Phi(x))$ is defined as:

$$M_i(\Phi(x)) = \begin{cases} 1, & \text{if } x \in \Omega_i \\ 0, & \text{else.} \end{cases} \tag{31}$$

For instance, in the four-phase case, $k = 2$ and $M_1 = H(\phi_1)H(\phi_2)$, $M_2 = H(\phi_1)(1 - H(\phi_2))$, $M_3 = (1 - H(\phi_1))H(\phi_2)$, $M_4 = (1 - H(\phi_1))(1 - H(\phi_2))$.

3) NUMERICAL IMPLEMENTATION

In order to solve Eq. 16 and Eq. 25 numerically on a computer, the central difference and the forward difference are used in this paper. Specifically, the level set $\phi(x, t)$ is discretized over a mesh using grid spacing interval h and time step Δt.

Then, we approximate the Heaviside function H (defined in Eq 6) and the Dirac delta function $\delta(\phi) = \frac{d}{d\phi}H(\phi)$ as follows:

$$H_\varepsilon(\phi) = \frac{1}{2}\left[1 + \frac{2}{\pi}\arctan\left(\frac{\phi}{\varepsilon}\right)\right], \tag{32}$$

$$\delta_\varepsilon(\phi) = \frac{1}{\pi}\frac{\varepsilon}{\varepsilon^2 + \phi^2}. \tag{33}$$

The detailed steps of LaG_ACM are shown in Algorithm 1. $L(\phi)$ is the length of the level set ϕ. m is a non-negative constant to terminate the curve evolution. ϕ^i is the evolving curve at the ith iteration.

IV. EXPERIMENTS

The performance of the proposed LaG_ACM is evaluated in this section. All the experiments are implemented in Matlab R2017b on a PC with Intel Core i7 3.4 GHz CPU, 24 GB RAM, and Windows 7 operating system. Besides, we fix the parameters $\Delta t = 0.1$, $h = 1$, $\varepsilon = 1$ and $\nu = 1$, in all experiments.

A. DATASETS

Since specialized datasets are not available for evaluating segmentation results using active contour models, we use the
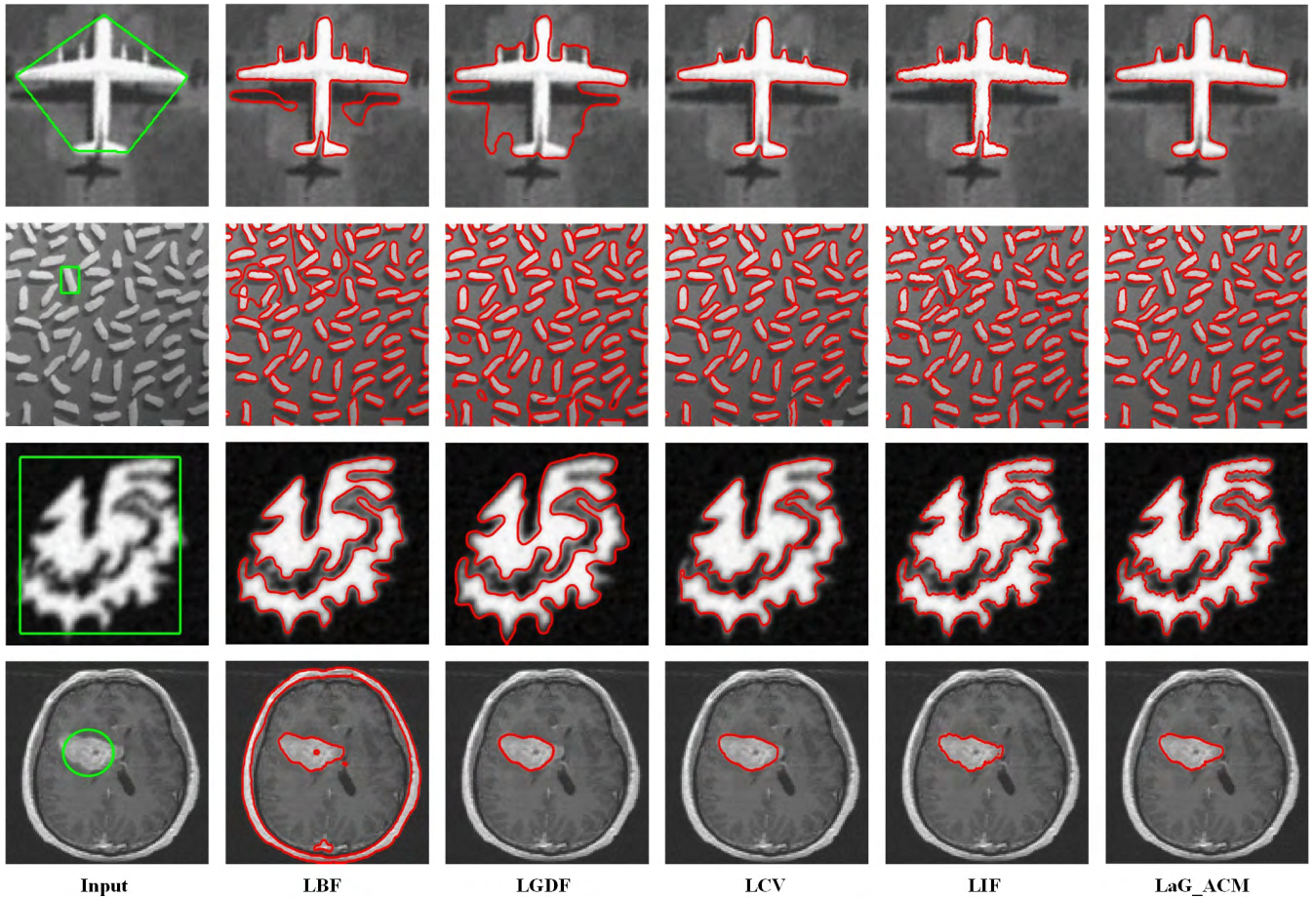
FIGURE 7. Segmentation results for two natural images and two medical images. From left to right: original images with corresponding initial contours (the green lines), segmentation results using the LBF [36], the LGDF [38], the LCV [39], the LIF [40] and the LaG_ACM, respectively.
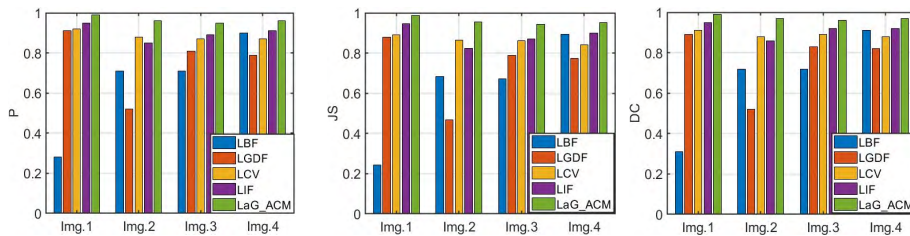

FIGURE 8. Illustration of P, JS and DC values for images shown in Fig. 7, respectively.

images appeared in previous papers based on active contour mode to conduct comparison experiments. Besides, to facilitate future research in the direction of active contour model and to more comprehensively evaluate the proposed method, we also conduct comparison experiments on some images in dataset MRSA-10K [64], [65], which is designed for saliency detection methods. We do not use all the images in the dataset since many images are not suitable for active contour models. Furthermore, we also use the brain Magnetic Resonance Images dataset [66] to evaluate the proposed method for segmenting medical images.

B. EVALUATION MEASURES

To quantitatively analyze the final segmentation results, several commonly used evaluation measures in the field of

pattern recognition and machine learning are used in this paper. In particular, as shown in Table 1, three measures are used to evaluate segmentation accuracy: Precision (P), Jaccard similarity (JS) and Dice coefficient (DC). The arrow symbol ↑ shown in the table means that, the larger the measure, the better the accuracy.

C. MODEL EVALUATION AND PERFORMANCE COMPARISON

In the following subsections, effectiveness assessments and comparison experiments are conducted on images with different degrees of intensity inhomogeneity, for example, synthetic images, natural images, medical images, remote sensing images, infrared images and sonar images to validate
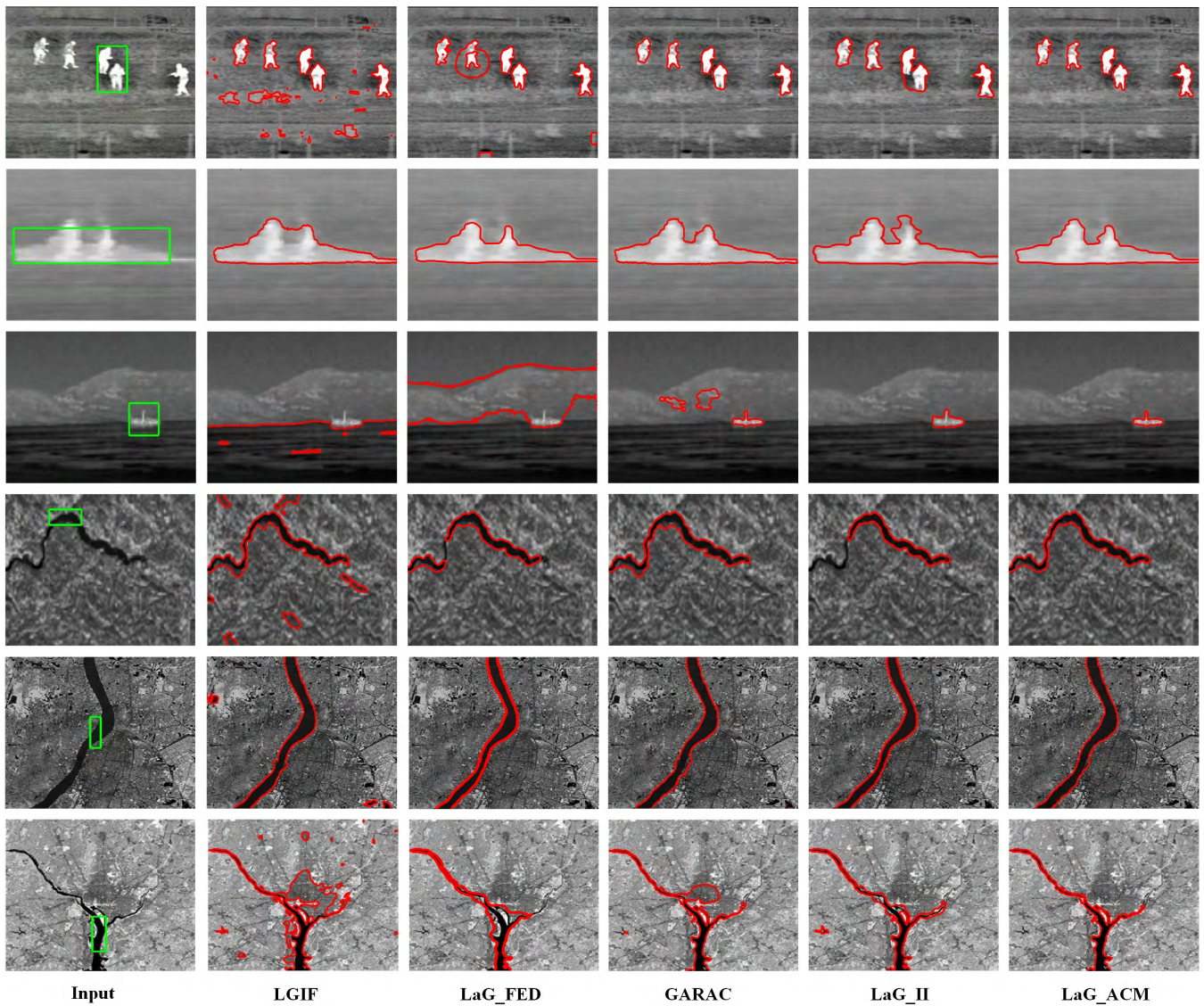
FIGURE 9. Comparison experiments on three infrared images and three remote sensing images with local and global ACMs. From left to right: original images with corresponding initial contours (the green lines), segmentation results of the LGIF [49], the LaG_FED [50], the GARAC [53], the LaG_II [9] and the LaG_ACM, respectively.

the robustness to noise and to initialization, segmentation accuracy and segmentation efficiency of the proposed method LaG_ACM. For each compared method, we use the original parameter settings included in the source code.

1) ROBUSTNESS EVALUATION

The robustness to initialization is tested on two natural images and one medical image as shown in Fig. 3. The green lines denote different initial contours that can be set inside, outside or across the object edge with different shapes, and the red lines denote the final segmentation results. From the results, we see that the proposed method is robust to different initializations for images with intensity inhomogeneity.

Fig. 4 shows the segmentation results of our method for a synthetic image with different kinds of noise distributions.

TABLE 1. Definitions of evaluation measures.

Name	Definition	Description
Precision (↑)	$P = \dfrac{TP}{TP+FP}$	P represents precision, and TP, FP represent the true positive and false positive, respectively.
Jaccard similarity (↑)	$JS = \dfrac{|S_G \cap S_T|}{|S_G \cup S_T|}$	JS is used to evaluate the similarity between the ground truth region and the segmented region.
Dice coefficient (↑)	$DC = \dfrac{2|S_G \cap S_T|}{|S_G| + |S_T|}$	DC is used to evaluate the percentage of positive pixels both in the segmented region and the ground truth region.

Row 1 to Row 3 are, respectively, images corrupted with Gaussian noise, salt and pepper noise and speckle noise with different levels, which are obtained using the Matlab built-in
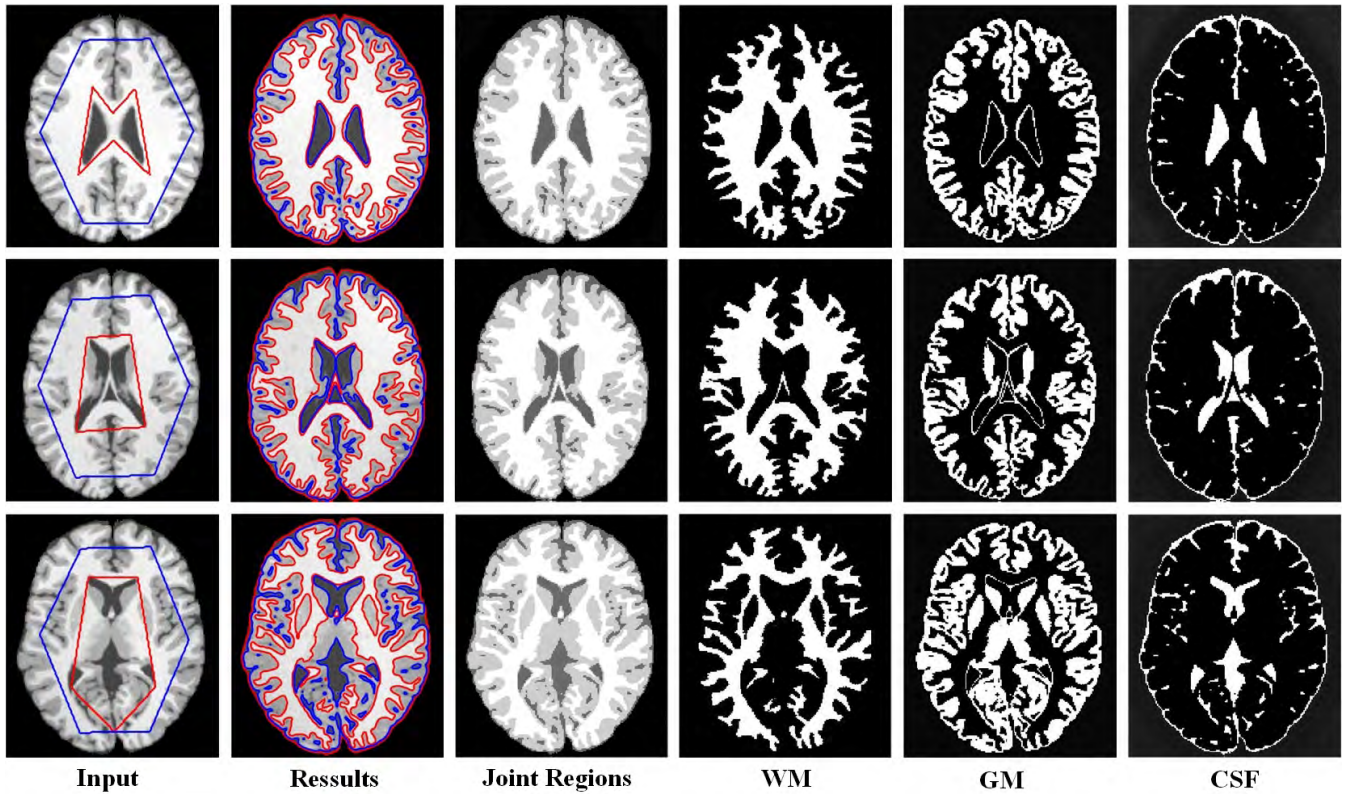
| Input | Ressults | Joint Regions | WM | GM | CSF |

FIGURE 10. From left to right: original images with initial contours of two level set functions: ϕ_1 and ϕ_2 (the red lines denotes ϕ_1, while the blue lines denotes ϕ_2), final segmentation results, joint segmentation regions, white matter (WM), gray matter (GM) and cerebrospinal fluid (CSF), using our method, respectively.
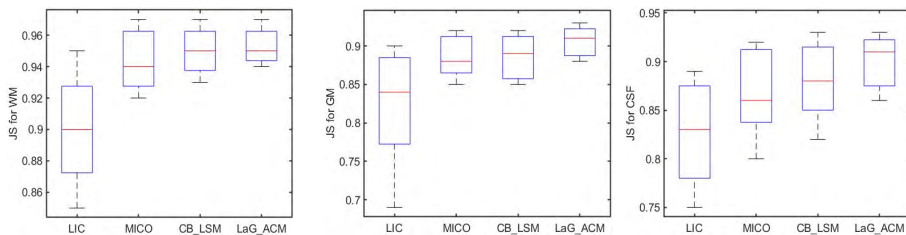

FIGURE 11. Comparison with bias field corrected ACMs: From left to right: the values of Jaccard similarity (JS) for WM, GM, and CSF using the LIC [60], the MICO [61], the CB_LSM [8] and the LaG_ACM, respectively.

function "imnoise" to add these noises to the original image. We observe that our method produces similar results at different noise levels for different kinds of noise distributions.

2) COMPARISON WITH EDGE-BASED ACMs

Since the DRLSE [22] model and the CV [29] model are famous for their segmentation speed in homogeneous images with strong edges, a comparison experiment with the DRLSE and the CV is conducted on six synthetic images used in previous papers to validate the segmentation speed of the LaG_ACM. As shown in Fig. 5, almost all the three models can accurately generate the segmentation except for the third image to the fifth image using the DRLSE method. Table 2 shows the corresponding running time and the number of iterations of each method. It can be observed that the

TABLE 2. Running time and number of iterations for images shown in Fig. 5.

Image	Number of iterations			Running time (in seconds)		
	DRLSE	CV	LaG_ACM	DRLSE	CV	LaG_ACM
Img.1	400	100	**25**	5.19	2.11	**1.27**
Img.2	250	60	**18**	3.70	1.71	**1.08**
Img.3	380	40	**18**	5.38	1.51	**1.06**
Img.4	350	40	**23**	4.49	1.57	**1.15**
Img.5	650	30	**11**	10.8	1.31	**0.78**
Img.6	450	34	**18**	4.67	1.45	**0.86**

proposed method is much faster than the other models since the weighting function can adaptively adjust the weight to accelerate the convergence.
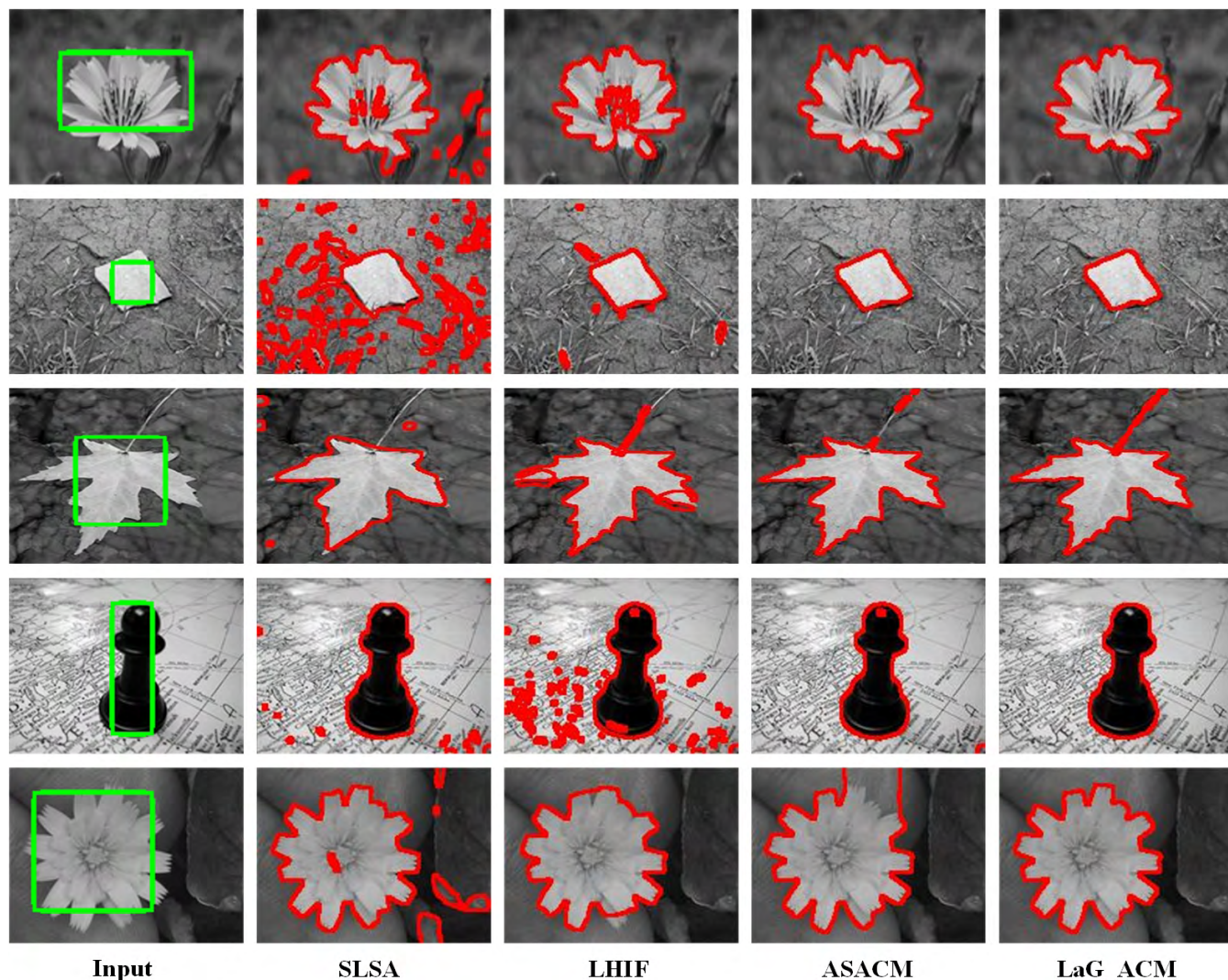
FIGURE 12. Comparison results on natural images. From left to right: original images with corresponding initial contours, segmentation results of SLSA [63], LHIF [56], ASACM [10] and LaG_ACM, respectively.

3) COMPARISON WITH LOCAL REGION-BASED ACMs

Fig. 6, shows the comparison results on four synthetic images with different degrees of intensity inhomogeneity between our method and four existing local region-based ACMs, the LBF [36], the LGDF [38], the LCV [39] and the LIF [40]. It can be seen that with the increase of the degree of image intensity inhomogeneity, the segmentation results using the other four methods become worse. Especially for the fourth image with severe intensity inhomogeneity, all the four methods fail to extract the correct contour of the object, which validates the conclusion mentioned in Section I that the local region-based ACMs are suitable for segmenting images with slight intensity inhomogeneity but not for images with severe intensity inhomogeneity. In contrast, the evolving curves of our method can always stop at the real edges of objects.

To further show the superior performance of our method, as shown in Fig. 7, another comparison experiment on two natural images and two medical images with the above four methods are conducted. The evaluation measures in Table 1 for segmenting the above images are shown in Fig. 8. We see that our proposed method gives higher segmentation accuracy compared to that of other models. This is because the local term of our model can accurately estimate the bias field and avoid the negative effects caused by it.

4) COMPARISON WITH HYBRID ACMs

In Fig. 9, we use three infrared images and three remote sensing images with severe intensity inhomogeneity to show the superiority of the proposed method compared to the LGIF [49], the LaG_FED [50], the GARAC [53], and the LaG_II [9]. From the segmentation results, we see that our method outperforms other methods, especially for the third and sixth images. For other images, the other four methods obtain over-segmentation or under-segmentation.
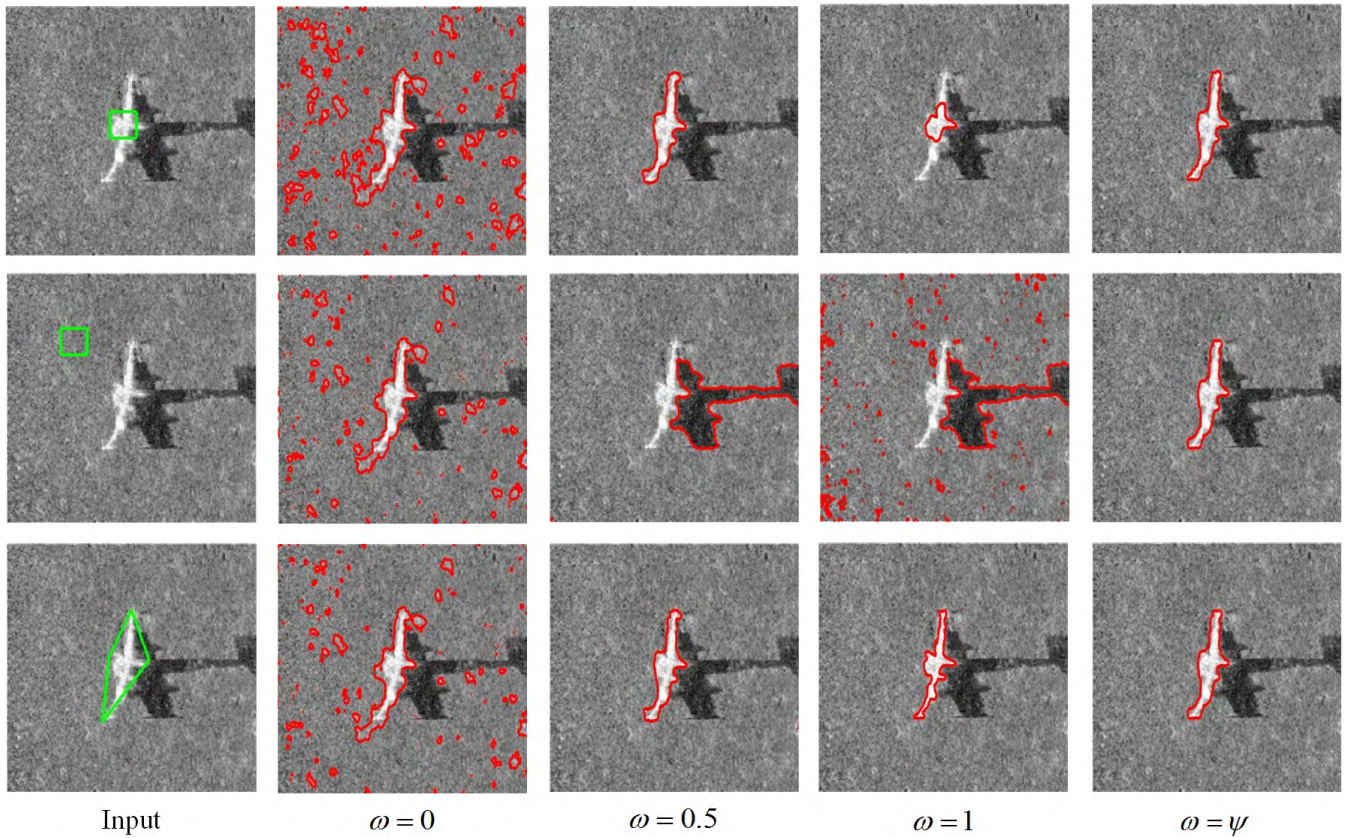
| Input | $\omega = 0$ | $\omega = 0.5$ | $\omega = 1$ | $\omega = \psi$ |

FIGURE 13. Comparison results on different weights. From left to right: original images with three different initial contours, segmentation results using *w* = 0, *w* = 0.5, *w* = 1 and *w* = Ψ, respectively.
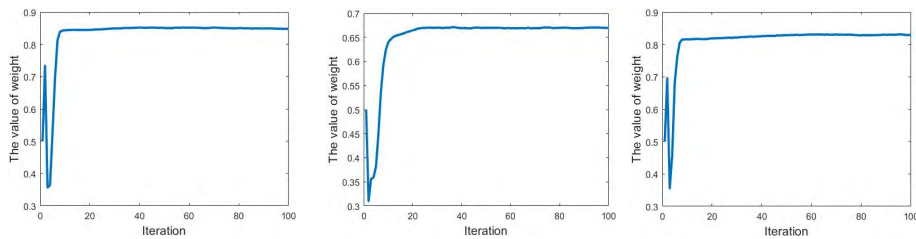

FIGURE 14. Illustration of the values of Ψ during segmentation of images shown in Fig. 13.

For example, the segmentation results of the second image using the LGIF and the LaG_II show that the region between the two chimneys (second row in Fig. 9) is under-segmented, and the segmentation result of the first image using the GARAC shows that the feet of the two persons on the right are over-segmented. Table 3 shows the evaluation measures. We observe that our method gives a higher segmentation accuracy compared to that of the other four models, because the local image bias field formulation can accurately extract the local intensity information and estimate the bias field.

Fig. 10 shows the joint segmentation results of brain Magnetic Resonance Images (MRI) [66], which consist of three types of tissues: white matter (WM), gray matter (GM) and cerebrospinal fluid (CSF). Considering one level func-

TABLE 3. The values of precision (P) for images shown in Fig. 9. The best results are shown in bold.

Method	Img.1	Img.2	Img.3	Img.4	Img.5	Img.6
LGIF [49]	0.52	0.90	0.01	0.74	0.90	0.44
LaG_FED [50]	0.75	0.95	0.22	0.90	0.95	0.81
GARAC [53]	0.94	0.97	0.47	0.92	0.96	0.79
LaG_II [9]	0.90	0.94	0.93	0.85	0.97	0.91
LaG_ACM	**0.97**	**0.98**	**0.96**	**0.93**	**0.98**	**0.94**

tion can only segment two types of tissues, we use two level set functions ϕ_1 and ϕ_2 according to Eq. 22 in this experiment. We observe that the proposed method success-
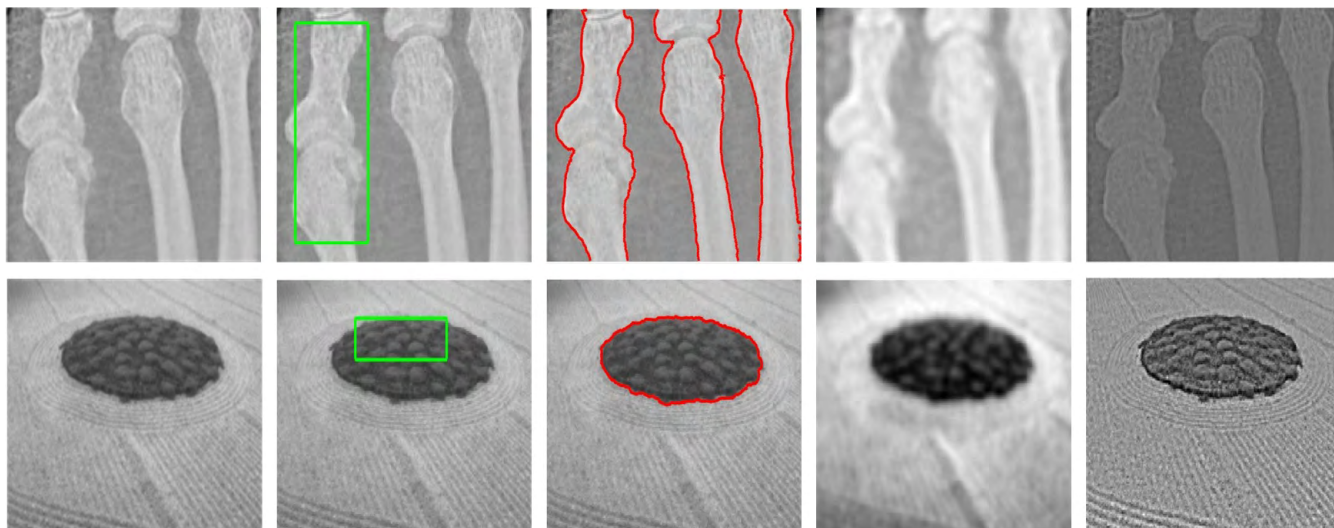
FIGURE 15. Bias-correction results on a medical image and a natural texture image. From left to right: original images, initial contours, final segmentation results, bias fields and corrected images, respectively.

fully extracts the three parts of the human brain. Fig. 11 shows the values of Jaccard similarity (JS) for WM, GM and CSF using the LIC [60], the MICO [61], the CB_LSM [8] and the LaG_ACM, respectively. It can be seen that our method performs better than the other methods for brain MRI segmentation.

5) COMPARISON WITH THE STATE-OF-THE-ART ACMs
To further evaluate the proposed method, we compare our method with three state-of-the-art methods including the local hybrid image fitting (LHIF) model [56], the SLSA model [63] and the ASACM model [10] on images of MRSA-10K [64], [65] as shown in Fig. 12. The segmentation results show that the three state-of-the-art methods obtain over-segmentation and under-segmentation. In contrast, our method can always accurately segment the four severe inhomogeneous images since our local term can accurately evaluate the bias field and avoid the negative effects. In addition, the defined weighting function can achieve better regularization than our previous method ASACM and obtain better performance.

D. ABLATION ANALYSIS
1) EFFECTIVENESS OF THE WEIGHTING FUNCTION
In Fig. 13, the effectiveness of the weighting function Ψ is validated on a sonar image with severe intensity inhomogeneity by comparing the segmentation results using a fixed weight and a weighting function Ψ. From the segmentation results using only the local term shown in the fourth column, we see that the local term has low robustness to initialization since different initializations give different segmentation results. Although the integration of the local term and the global term improves the performance of the model, it still cannot guarantee accuracy since the weight may not be set properly, which can be seen from the results in

the third column. In contrast, using the adaptive weighting function Ψ, the LaG_ACM achieves consistent final segmentation results for different initialization as shown in the fifth column. Fig. 14 shows the values of Ψ during segmentation. In addition to improving accuracy, Ψ also improves the segmentation efficiency.

2) EFFECTIVENESS OF THE BIAS FIELD TERM
Fig. 15 shows the bias-corrected results on a medical image and a natural texture image using our method. From the fourth and the fifth columns, we see that b in Eq. 8 successfully estimates the bias field and avoids the influence of intensity inhomogeneity. To more clearly show the difference between the original images and the corrected images, their histograms are shown in Fig. 16.
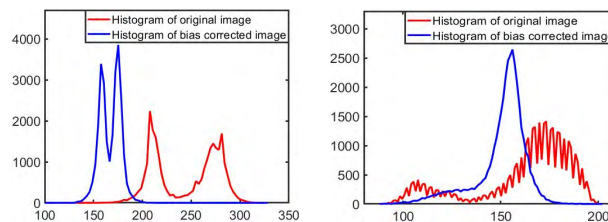

FIGURE 16. Histograms for images shown in Fig. 15.

V. CONCLUSIONS
In this paper, we propose a novel local and global ACM (LaG_ACM) for segmenting images with intensity inhomogeneity. Specifically, we first construct a global fitting image formulation and define a novel global term based on relative entropy between the original images and the global fitting image formulation to enable the proposed method to be robust to noise and to initialization. Then, by integrating the proposed local bias field fitting images formulation with

the active contour model, a local term based on the mean squared error is defined, which helps to estimate the bias field and eliminate the influence of the inherent intensity inhomogeneity of the original image. More importantly, we propose a novel weighting function based on image entropy to adaptively adjust the weight between the two terms, which significantly improves the segmentation speed. Finally, our method is evaluated by segmenting different types of inhomogeneous images. Comparison experiments with state-of-the-art models also validate the performance of the proposed method.

One shortcoming of the proposed method is that it performs poorly in segmenting color images [67] since it only uses intensity information to construct the energy function. In the future, we plan to tackle such an interesting problem.

APPENDIX

For two-phase level set, the minimization of the energy function $E^{LaG\_ACM}(\phi)$ in Eq. 16 and Eq. 25 is equivalent to solving the steady-state solution of the gradient flow equation as bellow:

$$\frac{\partial \phi}{\partial t} = -\frac{\partial E^{LaG\_ACM}}{\partial \phi},$$

where $\frac{\partial E^{LaG\_ACM}}{\partial \phi} = \frac{\partial E^G}{\partial \phi} + \frac{\partial E^L}{\partial \phi} + \frac{\partial E^R}{\partial \phi}$ is the Gâteaux derivative of the global term E^G, the local term E^L and the regularization term E^R. To solve them, we first add the variation η to the level set function ϕ: $\tilde{\phi} = \phi + \varepsilon\eta$. Then, keeping all the other parameters c_i, b, θ_i fixed, we can get:

$$\frac{\partial E^G(\phi)}{\partial \phi} = \lim_{\varepsilon \to 0}\left[\frac{\partial}{\partial \varepsilon}\int_{\Omega}\left(I(x)\log\frac{I(x)}{I^{GFI}(x)}\right.\right.$$
$$\left.\left. + I^{GFI}(x)\log\frac{I^{GFI}(x)}{I(x)}\right)dx\right]$$
$$= \lim_{\varepsilon \to 0}\left[\int_{\Omega}\left(-\frac{I(x)}{I^{GFI}(x)} + 1 + \log\frac{I^{GFI}(x)}{I(x)}\right)\right.$$
$$\left. \times (c_1 - c_2)\eta\delta_\varepsilon(\tilde{\phi})\, dx\right]$$
$$= \int_{\Omega}\left(-\frac{I(x)}{I^{GFI}(x)} + 1 + \log\frac{I^{GFI}(x)}{I(x)}\right)$$
$$\times (c_1 - c_2)\eta\delta_\varepsilon(\phi)\, dx,$$
$$\frac{\partial E^L(\phi)}{\partial \phi} = \lim_{\varepsilon \to 0}\left(\frac{\partial}{\partial \varepsilon}\frac{1}{2}\int\int |I(x) - I^{LIBF}(x)|^2\, dxdy\right)$$
$$= \lim_{\varepsilon \to 0}\left(-\int (I(x) - I^{LIBF}(x))(\theta_1 - \theta_2)\right.$$
$$\left. \times (b \otimes w)\eta\delta_\varepsilon(\tilde{\phi})\, dx\right)$$
$$= -\int\left((I(x) - I^{LIBF}(x))(\theta_1 - \theta_2)\right.$$
$$\left. \times (b \otimes w)\eta\delta_\varepsilon(\phi)\right)dx.$$

Since $\frac{\partial E^R(\phi)}{\partial \phi}$ has been already analyzed in [22], we will not go into them. So the Euler-Lagrange equation can be obtained:

$$(1 - \Psi)\left(-\frac{I(x)}{I^{GFI}(x)} + 1 + \log\frac{I^{GFI}(x)}{I(x)}\right)(c_1 - c_2)\delta_\varepsilon(\phi)$$
$$- \Psi(I(x) - I^{LIBF}(x))(\theta_1 - \theta_2)(b \otimes w)\delta_\varepsilon(\phi)$$
$$- v\delta_\varepsilon(\phi)\text{div}\left(\frac{\nabla\phi}{|\nabla\phi|}\right) - u\text{div}(d_p(|\nabla\phi|)\nabla\phi) = 0.$$

Finally, we can obtain the gradient descent flow as follows:

$$\frac{\partial \phi}{\partial t} = \delta_\varepsilon(\phi)((1 - \Psi)\alpha_1 + \Psi\alpha_2) + v\delta_\varepsilon(\phi)\text{div}\left(\frac{\nabla\phi}{|\nabla\phi|}\right)$$
$$+ u\text{div}(d_p(|\nabla\phi|)\nabla\phi),$$
$$\alpha_1 = \left(\frac{I(x)}{I^{GFI}(x)} - 1 - \log\frac{I^{GFI}(x)}{I(x)}\right)(c_1 - c_2),$$
$$\alpha_2 = (I(x) - I^{LIBF}(x))(\theta_1 - \theta_2)(b \otimes w).$$

The multi-phase case can be derived similarly.

REFERENCES

[1] D. Singh and C. K. Mohan, "Graph formulation of video activities for abnormal activity recognition," *Pattern Recognit.*, vol. 65, pp. 265–272, May 2017.

[2] M. Gong, Y. Qian, and L. Cheng, "Integrated foreground segmentation and boundary matting for live videos," *IEEE Trans. Image Process.*, vol. 24, no. 4, pp. 1356–1370, Apr. 2015.

[3] Y. Qian, M. Gong, and L. Cheng, "STOCS: An efficient self-tuning multiclass classification approach," in *Proc. Can. Conf. Artif. Intell.* Cham, Switzerland: Springer, 2015, pp. 291–306.

[4] Y. Qian, H. Yuan, and M. Gong, "Budget-driven big data classification," in *Proc. Can. Conf. Artif. Intell.* Cham, Switzerland: Springer, 2015, pp. 71–83.

[5] S. Yin, Y. Zhang, and S. Karim, "Large scale remote sensing image segmentation based on fuzzy region competition and Gaussian mixture model," *IEEE Access*, vol. 6, pp. 26069–26080, 2018.

[6] M. Pinheiro and J. L. Alves, "A new level-set-based protocol for accurate bone segmentation from CT imaging," *IEEE Access*, vol. 3, pp. 1894–1906, 2015.

[7] B. N. Li, J. Qin, R. Wang, M. Wang, and X. Li, "Selective level set segmentation using fuzzy region competition," *IEEE Access*, vol. 4, pp. 4777–4788, Aug. 2016.

[8] S. Zhou, J. Wang, M. Zhang, Q. Cai, and Y. Gong, "Correntropy-based level set method for medical image segmentation and bias correction," *Neurocomputing*, vol. 234, pp. 216–229, Apr. 2017.

[9] S. Zhou, J. Wang, S. Zhang, Y. Liang, and Y. Gong, "Active contour model based on local and global intensity information for medical image segmentation," *Neurocomputing*, vol. 186, pp. 107–118, Apr. 2016.

[10] Q. Cai, H. Liu, S. Zhou, J. Sun, and J. Li, "An adaptive-scale active contour model for inhomogeneous image segmentation and bias field estimation," *Pattern Recognition*, vol. 82, pp. 79–93, Oct. 2018.

[11] M. Kass, A. Witkin, and D. Terzopoulos, "Snakes: Active contour models," *Int. J. Comput. Vis.*, vol. 1, no. 4, pp. 321–331, 1988.

[12] V. Caselles, F. Catté, T. Coll, and F. Dibos, "A geometric model for active contours in image processing," *Numer. Math.*, vol. 66, no. 1, pp. 1–31, 1993.

[13] R. Malladi, J. A. Sethian, and B. C. Vemuri, "Shape modeling with front propagation: A level set approach," *IEEE Trans. Pattern Anal. Mach. Intell.*, vol. 17, no. 2, pp. 158–175, Feb. 1995.

[14] S. Kichenassamy, A. Kumar, P. Olver, A. Tannenbaum, and A. Yezzi, "Gradient flows and geometric active contour models," in *Proc. IEEE Int. Conf. Comput. Vis.*, Jun. 1995, pp. 810–815.

[15] K. Siddiqi, Y. B. Lauziere, A. Tannenbaum, and S. W. Zucker, "Area and length minimizing flows for shape segmentation," *IEEE Trans. Image Process.*, vol. 7, no. 3, pp. 433–443, Mar. 1998.

[16] W.-P. Choi, K.-M. Lam, and W.-C. Siu, "An adaptive active contour model for highly irregular boundaries," *Pattern Recognit.*, vol. 34, no. 2, pp. 323–331, 2001.

[17] V. Caselles, R. Kimmel, and G. Sapiro, "Geodesic active contours," *Int. J. Comput. Vis.*, vol. 22, no. 1, pp. 61–79, 1997.

[18] A. Vasilevskiy and K. Siddiqi, "Flux maximizing geometric flows," *IEEE Trans. Pattern Anal. Mach. Intell.*, vol. 24, no. 12, pp. 1565–1578, Dec. 2002.

[19] N. Paragios and R. Deriche, "Geodesic active regions and level set methods for supervised texture segmentation," *Int. J. Comput. Vis.*, vol. 46, no. 3, pp. 223–247, Feb. 2002.

[20] C. Li, C. Xu, C. Gui, and M. D. Fox, "Level set evolution without re-initialization: A new variational formulation," in *Proc. IEEE Comput. Soc. Conf. Comput. Vis. Pattern Recognit.*, vol. 1, Jun. 2005, pp. 430–436.

[21] C. Le Guyader and C. Gout, "Geodesic active contour under geometrical conditions: Theory and 3D applications," *Numer. Algorithms*, vol. 48, nos. 1–3, pp. 105–133, 2008.

[22] C. Li, C. Xu, C. Gui, and M. D. Fox, "Distance regularized level set evolution and its application to image segmentation," *IEEE Trans. Image Process.*, vol. 19, no. 12, pp. 3243–3254, Dec. 2010.

[23] X. Gao, B. Wang, D. Tao, and X. Li, "A relay level set method for automatic image segmentation," *IEEE Trans. Syst. Man, Cybern. B, Cybern.*, vol. 41, no. 2, pp. 518–525, Apr. 2011.

[24] S. Balla-Arabé, X. Gao, and B. Wang, "A fast and robust level set method for image segmentation using fuzzy clustering and lattice Boltzmann method," *IEEE Trans. Cybern.*, vol. 43, no. 3, pp. 910–920, Jun. 2013.

[25] L. Mabood, H. Ali, N. Badshah, K. Chen, and G. A. Khan, "Active contours textural and inhomogeneous object extraction," *Pattern Recognit.*, vol. 55, pp. 87–99, Jul. 2016.

[26] C. Liu, W. Liu, and W. Xing, "An improved edge-based level set method combining local regional fitting information for noisy image segmentation," *Signal Process.*, vol. 130, pp. 12–21, Jan. 2017.

[27] D. Mumford and J. Shah, "Optimal approximations by piecewise smooth functions and associated variational problems," *Commun. Pure Appl. Math.*, vol. 42, no. 5, pp. 577–685, 1989.

[28] M. Gobbino, "Finite difference approximation of the Mumford-Shah functional," *Commun. Pure Appl. Math.*, vol. 51, no. 2, pp. 197–228, 1998.

[29] T. F. Chan and L. A. Vese, "Active contours without edges," *IEEE Trans. Image Process.*, vol. 10, no. 2, pp. 266–277, Feb. 2001.

[30] T. F. Chan and L. A. Vese, "A level set algorithm for minimizing the Mumford-Shah functional in image processing," in *Proc. IEEE Workshop Variational Level Set Methods Comput. Vis.*, Jul. 2001, pp. 161–168.

[31] L. A. Vese and T. F. Chan, "A multiphase level set framework for image segmentation using the Mumford and Shah model," *Int. J. Comput. Vis.*, vol. 50, no. 3, pp. 271–293, Dec. 2002.

[32] S. Esedoḡlu and Y.-H. R. Tsai, "Threshold dynamics for the piecewise constant Mumford–Shah functional," *J. Comput. Phys.*, vol. 211, no. 1, pp. 367–384, 2006.

[33] J. Lie, M. Lysaker, and X.-C. Tai, "A binary level set model and some applications to Mumford-Shah image segmentation," *IEEE Trans. Image Process.*, vol. 15, no. 5, pp. 1171–1181, May 2006.

[34] L. Grady and C. V. Alvino, "The piecewise smooth Mumford–Shah functional on an arbitrary graph," *IEEE Trans. Image Process.*, vol. 18, no. 11, pp. 2547–2561, Nov. 2009.

[35] T. Pock, D. Cremers, H. Bischof, and A. Chambolle, "An algorithm for minimizing the Mumford-Shah functional," in *Proc. IEEE Int. Conf. Comput. Vis.*, Sep./Oct. 2009, pp. 1133–1140.

[36] C. Li, C.-Y. Kao, J. C. Gore, and Z. Ding, "Implicit active contours driven by local binary fitting energy," in *Proc. IEEE Conf. Comput. Vis. Pattern Recognit.*, Jun. 2007, pp. 1–7.

[37] C. Li, C.-Y. Kao, J. C. Gore, and Z. Ding, "Minimization of region-scalable fitting energy for image segmentation," *IEEE Trans. Image Process.*, vol. 17, no. 10, pp. 1940–1949, Oct. 2008.

[38] L. Wang, L. He, A. Mishra, and C. Li, "Active contours driven by local Gaussian distribution fitting energy," *Signal Process.*, vol. 89, no. 12, pp. 2435–2447, 2009.

[39] X.-F. Wang, D.-S. Huang, and H. Xu, "An efficient local Chan–Vese model for image segmentation," *Pattern Recognit.*, vol. 43, no. 3, pp. 603–618, 2010.

[40] K. Zhang, H. Song, and L. Zhang, "Active contours driven by local image fitting energy," *Pattern Recognit.*, vol. 43, no. 4, pp. 1199–1206, Apr. 2010.

[41] S. Liu and Y. Peng, "A local region-based Chan–Vese model for image segmentation," *Pattern Recognit.*, vol. 45, no. 7, pp. 2769–2779, Jul. 2012.

[42] Y. Wang, S. Xiang, C. Pan, L. Wang, and G. Meng, "Level set evolution with locally linear classification for image segmentation," *Pattern Recognit.*, vol. 46, no. 6, pp. 1734–1746, Jun. 2013.

[43] X.-F. Wang, H. Min, and Y.-G. Zhang, "Multi-scale local region based level set method for image segmentation in the presence of intensity Inhomogeneity," *Neurocomputing*, vol. 151, pp. 1086–1098, Mar. 2015.

[44] T. H. N. Le and M. Savvides, "A novel shape constrained feature-based active contour model for lips/mouth segmentation in the wild," *Pattern Recognit.*, vol. 54, pp. 23–33, Jun. 2016.

[45] X.-F. Wang, H. Min, L. Zou, Y.-G. Zhang, Y.-Y. Tang, and C.-L. P. Chen, "An efficient level set method based on multi-scale image segmentation and Hermite differential operator," *Neurocomputing*, vol. 188, pp. 90–101, May 2016.

[46] Y. Wu and C. He, "Indirectly regularized variational level set model for image segmentation," *Neurocomputing*, vol. 171, pp. 194–208, Jan. 2016.

[47] Y. Song, Y. Wu, and Y. Dai, "A new active contour remote sensing river image segmentation algorithm inspired from the cross entropy," *Digit. Signal Process.*, vol. 48, pp. 322–332, Jan. 2016.

[48] B. Han and Y. Wu, "A novel active contour model based on modified symmetric cross entropy for remote sensing river image segmentation," *Pattern Recognit.*, vol. 67, pp. 396–409, Jul. 2017.

[49] L. Wang, C. Li, Q. Sun, D. Xia, and C.-Y. Kao, "Active contours driven by local and global intensity fitting energy with application to brain MR image segmentation," *Comput. Med. Imag. Graph.*, vol. 33, no. 7, pp. 520–531, 2009.

[50] Y. Yu, C. Zhang, Y. Wei, and X. Li, "Active contour method combining local fitting energy and global fitting energy dynamically," in *Proc. Int. Conf. Med. Biometrics*. Berlin, Germany: Springer, 2010, pp. 163–172.

[51] L. Liu, Q. Zhang, M. Wu, W. Li, and F. Shang, "Adaptive segmentation of magnetic resonance images with intensity inhomogeneity using level set method," *Magn. Reson. Imag.*, vol. 31, no. 4, pp. 567–574, 2013.

[52] X.-F. Wang, H. Min, L. Zou, and Y.-G. Zhang, "A novel level set method for image segmentation by incorporating local statistical analysis and global similarity measurement," *Pattern Recognit.*, vol. 48, no. 1, pp. 189–204, 2015.

[53] H. Wang, T.-Z. Huang, Z. Xu, and Y. Wang, "A two-stage image segmentation via global and local region active contours," *Neurocomputing*, vol. 205, pp. 130–140, Sep. 2016.

[54] X.-F. Wang, L. Zou, L.-X. Xu, G. Lv, and C. Tang, "Hybrid level set method based on image diffusion," *Neurocomputing*, vol. 228, pp. 53–64, Mar. 2017.

[55] L. Zhang, X. Peng, G. Li, and H. Li, "A novel active contour model for image segmentation using local and global region-based information," *Mach. Vis. Appl.*, vol. 28, nos. 1–2, pp. 75–89, 2017.

[56] L. Wang, Y. Chang, H. Wang, Z. Wu, J. Pu, and X. Yang, "An active contour model based on local fitted images for image segmentation," *Inf. Sci.*, vol. 418, pp. 61–73, Mar. 2017.

[57] Y. Chen, X. Yue, R. Y. Da Xu, and H. Fujita, "Region scalable active contour model with global constraint," *Knowl.-Based Syst.*, vol. 120, pp. 57–73, Mar. 2017.

[58] B. Han and Y. Wu, "A hybrid active contour model driven by novel global and local fitting energies for image segmentation," *Multimedia Tools Appl.*, vol. 77, pp. 1–16, May 2018.

[59] C. Li, C. Xu, A. W. Anderson, and J. C. Gore, "MRI tissue classification and bias field estimation based on coherent local intensity clustering: A unified energy minimization framework," in *Proc. Int. Conf. Inf. Process. Med. Imag.* Berlin, Germany: Springer, 2009, pp. 288–299.

[60] C. Li, R. Huang, Z. Ding, J. C. Gatenby, D. N. Metaxas, and J. C. Gore, "A level set method for image segmentation in the presence of intensity inhomogeneities with application to MRI," *IEEE Trans. Image Process.*, vol. 20, no. 7, pp. 2007–2016, Jul. 2011.

[61] C. Li, J. C. Gore, and C. Davatzikos, "Multiplicative intrinsic component optimization (MICO) for MRI bias field estimation and tissue segmentation," *Magn. Reson. Imag.*, vol. 32, no. 7, pp. 913–923, Sep. 2014.

[62] K. Zhang, Q. Liu, H. Song, and X. Li, "A variational approach to simultaneous image segmentation and bias correction," *IEEE Trans. Cybern.*, vol. 45, no. 8, pp. 1426–1437, Aug. 2015.

[63] K. Zhang, L. Zhang, K.-M. Lam, and D. Zhang, "A level set approach to image segmentation with intensity inhomogeneity," *IEEE Trans. Cybern.*, vol. 46, no. 2, pp. 546–557, Feb. 2016.

[64] T. Liu *et al.*, "Learning to detect a salient object," *IEEE Trans. Pattern Anal. Mach. Intell.*, vol. 33, no. 2, pp. 353–367, Feb. 2011.

[65] M.-M. Cheng, N. J. Mitra, X. Huang, P. H. S. Torr, and S.-M. Hu, "Global contrast based salient region detection," *IEEE Trans. Pattern Anal. Mach. Intell.*, vol. 37, no. 3, pp. 569–582, Mar. 2015.

[66] C. A. Cocosco, V. Kollokian, R. K.-S. Kwan, G. B. Pike, and A. C. Evans, "BrainWeb: Online interface to a 3D MRI simulated brain database," *NeuroImage*, vol. 5, p. 425, Feb. 1997.

[67] S. Yin, Y. Qian, and M. Gong, "Unsupervised hierarchical image segmentation through fuzzy entropy maximization," *Pattern Recognit.*, vol. 68, pp. 245–259, Aug. 2017.

QING CAI received the M.E. degree from the Department of Automation, Northwestern Polytechnical University, Xi'an, China, in 2016, where he is currently pursuing the Ph.D. degree. His main research interests include image segmentation, target tracking, deep learning, and machine learning.

HUIYING LIU received the B.E., M.E., and Ph.D. degrees from Northwestern Polytechnical University, Xi'an, China, in 1981, 2000, and 2007, respectively. She was a Senior Visiting Scholar with Clyde University from 2003 to 2004. Since 1996, she has been a Professor with the Department of Automation, Northwestern Polytechnical University. She is currently the Deputy Director of the Department of Systems Engineering, Shaanxi Institute of Automation. Her research interests cover a wide range of topics from computer science to computer vision, which include system modeling and simulation, image processing and image recognition, pedestrian detection, single-target tracking, and multi-target tracking. She has published over 60 papers in international journals and conference. She has completed more than 20 important research projects and funds, including the National Natural Science Foundation, the "863" Project, the General Armament Department Project, and the Aviation Science Fund. She received a Third Prize of scientific and technological progress of the National Defense Science and Technology Commission, a Second Prize of Shaanxi Province teaching achievement, the Northwestern Polytechnic University Teaching Achievement Award, and other awards more than 20 items.

YIMING QIAN received the B.E. degree from the University of Science and Technology of China, Hefei, China, in 2012, and the M.Sc. degree from the Memorial University of New-foundland, St. John's, Canada, in 2014. He is currently pursuing the Ph.D. degree with the Department of Computing Science, University of Alberta, Edmonton, Canada. His research interests include machine learning and computer vision.

JING LI received the B.E., M.E., and Ph.D. degrees from Northwestern Polytechnical University, Xi'an, China, in 2004, 2007, and 2013, respectively. She was a joint Training Doctor at the University of California at Berkeley from 2008 to 2010. She is currently an Associate Professor with the Department of Mechanical Engineering, Northwestern Polytechnical University. She has published about 20 conference and journal papers. Her research interests are in biological signal detection, evaluation, flight control simulation, and image processing.

XIAOJUN DUAN (M'06) received the B.E., M.E., and Ph.D. degrees from Northwestern Polytechnical University, Xi'an, China, in 2002, 2004, and 2010, respectively. He was with the UAV industry for 15 years, mainly involved in flight control, navigation vision guidance, avionics, and simulation testing technology research. He is currently a Professor with Northwestern Polytechnical University. His research directions include navigation guidance and control, flight simulation and testing, redundancy management, and airborne embedded software. He is a member of IAA.

YEE-HONG YANG (SM'91) received the B.Sc. degree (Hons.) from The University of Hong Kong, the M.Sc. degree from Simon Fraser University, and the M.S.E.E. and Ph.D. degrees from the University of Pittsburgh. He was a Faculty Member with the Department of Computer Science, University of Saskatchewan, from 1983 to 2001, and served as a Graduate Chair from 1999 to 2001. While there, in addition to department level committees, he also served on many college and university level committees. Since 2001, he has been a Professor with the Department of Computing Science, University of Alberta, where he served as an Associate Chair (Graduate Studies) from 2003 to 2005. He has published over 100 papers in international journals and conference proceedings in the areas of computer vision and graphics. His research interests cover a wide range of topics from computer graphics to computer vision, which include physically based animation of Newtonian and non-Newtonian fluids, texture analysis and synthesis, human body motion analysis and synthesis, computational photography, stereo and multiple view computer vision, and underwater imaging. In addition to serving as a reviewer to numerous international journals, conferences, and funding agencies, he has served on the program committees of many national and international conferences. In 2007, he was invited to serve on the expert review panel to evaluate computer science research in Finland. He serves on the Editorial Board of the journal *Pattern Recognition*.

• • •